Physics – Uspekhi **63** (7) 683 – 697 (2020)

REVIEWS OF TOPICAL PROBLEMS PACS numbers: 92.10.ak, 92.60.Fm, 92.60.hk

Structure and dynamics of concentrated mesoscale vortices in planetary atmospheres

O G Onishchenko, O A Pokhotelov, N M Astaf'eva, W Horton, V N Fedun

DOI: https://doi.org/10.3367/UFNe.2019.07.038611

Contents

Abstract. Concentrated vortices are spatially localized structures with nonzero vorticity surrounded by a potential flow. These structures include a broad class of mesoscale vortices, such as dust devils, water vortices, and fire vortices, as well as larger-scale and more intense tornados. From a rather broad class of concentrated mesoscale vortices, dust devils are selected as the simplest and most easily observable structures owing to dust particles that play the role of tracers. The aim of this review is to present the main results of studies of dust devils in the atmospheres of Earth and Mars. In the framework of ideal fluid dynamics, a recently proposed model is discussed that allows describing vortex structures that are fully localized in space. The results of numerical modeling of vortex dynamics and an analytic model of vortex generation in a convectively unstable atmosphere are briefly discussed.

O G Onishchenko [1,2,a], **O A Pokhotelov** [1], **N M Astaf'eva** [2,b], **W Horton** [3,c], **V N Fedun** [4,d]
[1] Schmidt Institute of Physics of the Earth, Russian Academy of Sciences, ul. Bolshaya Gruzinskaya 10, 123242 Moscow, Russian Federation
[2] Space Research Institute, Russian Academy of Sciences, ul. Profsoyuznaya 84/32, 117997 Moscow, Russian Federation
[3] Applied Research Laboratory at the University of Texas (ARLUT), Austin, 78712, USA
[4] Department of Automatic Control and Systems Engineering, University of Sheffield, Sheffield S13JD, UK
E-mail: [a] onish@ifz.ru, [b] ast@iki.rssi.ru, [c] wendell.horton@gmail.com, [d] v.fedun@sheffield.ac.uk

Received 19 April 2019, revised 4 July 2019
Uspekhi Fizicheskikh Nauk **190** (7) 732 – 748 (2020)
Translated by S D Danilov; edited by A M Semikhatov

Keywords: vortices, model of vortices, nonlinear structures, ideal fluid dynamics

1. Introduction

Any real motion in the atmosphere is vortical to one or degree another. Furthermore, the existence of well pronounced vortical structures in the atmosphere is one of the main factors defining weather and climate, which are the result of interactions among vortices of various topologies and scales. Concentrated mesoscale vortices stand out among a great variety of vortical motions in the atmosphere, being of increased interest from the standpoint of both fundamental research and practice. Concentrated vortices (CVs) are nonstationary spatially localized vortical structures, elongated in the vertical direction, with a characteristic transverse size from several meters to several hundred meters. Concentrated vortices include dust devils (DDs), as well as more intense and larger-scale vortices — tornados [1–9]. In seas or large lakes, water jets (or waterspouts) are observed [10–12]. Distinct from dust whirlwinds, waterspouts entrain water droplets in vertical vortical motion. Furthermore, in fires during calm weather, fiery devils may suddenly occur. Although vortices in this class evolve in various media and, generally speaking, have different generation natures, they are all characterized by ascending helicoidal motion. This broad class of vortices attracts the attention of numerous researchers. The rotation velocity in CVs attains its maximum at the characteristic vortex radius and tends to zero at the periphery, which agrees well with the rotation velocity behavior in a stationary Rankine vortex [13–15]. Dust devils, as the simplest and rather frequently and easily observed structures, are of special interest for studying the whole class of atmospheric CVs.

Dust intake into the atmosphere is governed by numerous natural phenomena, the most powerful ones being sand (dust) storms and dust whirlwinds [16–21]. A substantial amount of aerosols in the atmosphere is related to dust storms, which carry dust far into the oceans and even transport it from Africa to America across the Atlantic Ocean. The effect of dust on atmospheric dynamics and energy exchange presents one of the least studied yet most important factors contributing to the formation of Earth's climate. Studying these interactions is fundamental for the prognosis of weather change and climate variability.

The aim of this review is to summarize the research results pertaining to the CVs in the atmosphere. The main focus is on dust whirlwinds (DDs). From the broad class of CVs, they are selected as the simplest and most lively discussed vortices in the scientific literature. The dynamics of vortices can be roughly separated into three stages: generation, the quasistationary regime, and decay. The last may be caused by increased viscous losses and the influence of friction in the surface layer. Our main focus is on the first two stages of vortex evolution.

In Section 2, we briefly discuss the process of dust entrainment by vortices and the electrodynamics of vortices related to the electrification of dust particles. The consideration is rather sketchy because the details of these important processes are outside the scope of this review.

In Section 3, we present some results of DD observations in the terrestrial and Martian atmospheres.

In Section 4, we discuss models of stationary vortices. Commonly, the stage when vortices are in a quasistationary state lasts longer than the generation and decay stages. The known theoretical models of stationary vortices by Rankine, Burgers, and Sullivan are briefly discussed. Even though none of these models fully covers the dynamics of CVs, all of them are still used to describe individual details of this complex natural phenomenon. For example, the simplest Rankine model is frequently used to interpret observations of not only dust whirlwinds but also more powerful and complex typhoons. In Section 4.2.5, we discuss a new model of a stationary localized vortex. This model corresponds to an exact solution of the Euler equations for an incompressible fluid, offering a description of three-dimensional vortex structures exponentially localized not only radially but also vertically.

Section 5 is devoted to the discussion of a model describing the generation of jets, characterized by a two-dimensional velocity field, and CVs in a stratified atmosphere. It is shown that in a convectively unstable atmosphere, the poloidal (radial and vertical) jet velocities grow exponentially with time. The presence of seeding of large-scale vertical vorticity in the atmosphere is the cause of the explosive generation of vertical vorticity and azimuthal velocity.

In Section 6 we briefly consider the results of numerical modeling of vortex dynamics in a convectively unstable atmosphere.

The conclusion (Section 7) briefly summarizes the main statements.

2. Characteristic features

2.1 Dust devils: columns of rising dust

Dust devils are the most widely disseminated vortex structures of the terrestrial atmosphere [9, 22, 23]. A gray column of dust frequently reaches up to the clouds. Pilots observe ascending air streams and dust whirlwinds sometimes at altitudes of several kilometers. In most cases, dust is an indicator of DDs, but in regions poor in dust and sand, such vortices are less noticeable and can even be invisible.

The vortices entrain dust from the surface of a planet as a result of so-called *saltation* [24–26]. Sinclair [14] proposed that the presence of dust in the near-surface atmospheric layer, the existence of regions where the ground temperature is anomalously high, and the presence of local obstructions to wind, triggering the formation of shear flows, are necessary conditions for the DD formation. DDs are usually not dangerous in and of themselves, but there is evidence that they have been the cause of aviation incidents in some regions on Earth [27]. An analysis of the database on incidents of the National Transportation Safety Board, USA, based on 97 cases indicates that DDs can be considered the most probable cause of aviation incidents.

2.2 Characteristic parameters

The history of DD observations already counts almost 160 years, beginning with study [1] in 1860. Later research [2, 9, 17–23, 25, 26] was also dedicated to observations of DDs and their description. Most DDs are observed on afternoons in dry, calm weather when the soil is well heated by solar radiation. Rising warm air creates a vortex with reduced pressure in its center [9, 20, 21]. The characteristic diameter of a DD is from several meters to several dozen meters, and they may reach from several hundred to even a thousand meters in height. They move with a speed close to that of unperturbed wind. Owing to the presence of dust, they look like mini-tornados to an outside observer. The role of DDs in convection, soil erosion, and sand transport in arid regions on Earth has been intensively studied for a long time [24, 28–32].

The direction of DD circulation depends only on the initial conditions during their onset, because their spatial scales are not large enough for the effect of the Coriolis force to be significant, as, for example, in Rossby wave vortices. Very often, vortices rotating in mutually opposite directions can be observed to take part in a forming DD group.

Balme and Greeley [9], having summarized the results of previous research, presented a review of characteristic DD parameters on Earth and Mars. Larger DDs have larger rotation speeds and larger vertical velocities [29]. The radial structure of DDs can be roughly split into three concentric domains [33]: *an external domain* with constant (or slowly radially varying) weak vorticity; *a narrow domain* where vorticity jumps abruptly and the vertical flow velocity is small, and *an internal domain* where the flow converging to the center is transformed into a vertically ascending flow with large vertical and toroidal velocities. Typical terrestrial DDs have diameters under 10 m and heights not larger than several hundred meters [9, 13, 14, 32–40]. DDs — atmospheric whirlwinds — are less dangerous than large-scale tornados. For this reason, studies of DDs for a long time were outside the mainstream of meteorological research. Interest in DDs increased substantially when it became known that there are much more powerful DDs on Mars than on Earth. The first indications of the existence of DDs on Mars were obtained in the 1970s aboard the Viking spacecraft of the National Aeronautics and Space Administration (NASA), orbiting Mars [9, 41]. Since then, the topic of DDs has been intensively discussed in the scientific literature and at conferences (see, e.g., [9, 21, 42, 43]).

2.3 Dust content of the atmosphere and climate

Despite the large and ever growing body of research devoted to dust transport [44–48], the effect of dust on Earth's climate system remains rather uncertain. Vortices with an ascending spiral flow lift dust to high altitudes. As a result, the dust carried by winds is transported over large distances, noticeably influencing global and regional climate [49–51]. The most intense DDs can carry dust to an altitude of 10 km, affecting the structure of tropospheric aerosols. The dust supply to the atmosphere is governed by numerous phenomena, the most powerful being sand (dust) storms on a synoptic scale ($\sim$ 1000 km). Vortices with a reduced pressure at the center, sucking dust and lifting it to high altitudes, may be the cause of dust storms on Mars [53]. Dust redistributes energy by scattering and absorbing solar and terrestrial radiation. This causes heating of the atmosphere, increasing the net precipitation, but cooling the surface. Dust aerosols serve as nuclei of water vapor transformation into the liquid phase (as condensation nuclei in clouds) and solid phase (as ice nuclei) [54, 55]. The interactions between dust and clouds are rather complicated and insufficiently studied [48, 54]. Furthermore, dust deposition on glaciers and snow cover reduces the albedo (the capability to reflect), which is the cause of warming and earlier snow melting [44–46, 56, 57]. Climate change is very sensitive to the global dust cycle: the global dust deposition rate during the glacial maximum is several times higher than during the interglacial epoch [47, 58, 59]. We note that an increase in dust deposition has been observed over the last 50 years [45, 60].

The role of DDs in the dry and dusty Martian atmosphere is even more important than on Earth [31, 61]. On Earth, DDs provide only 3.4% of the dust supply to the atmosphere [62], whereas on Mars their share is about 50% [63]. It is assumed in [64] that DDs may be present on Neptune's largest satellite Triton.

2.4 Saltation

The transport of sand, dust, or other substances governed by winds is an eolian process named after the Greek god of the winds, Aeolus. Eolian processes are observed not only on Earth but also on Mars, Venus, and Saturn's satellite Titan. On Earth, they mainly take place in deserts, on beaches, or in other regions with scarce vegetation. Winds blowing sand and dust in these regions change the surface, triggering the formation of sand dunes and ripples, soil degradation, and the transport of soil fragments [44–47, 57].

Saltation (from Latin saltus — a leap) is the process of suspending and transporting sand particles over a planet's surface by abrupt wind bursts. Hitting the surface, particles entrain other particles. The first thorough review of the physics of saltation was proposed by Bagnold in his book [16], laying the foundations of this branch of science. The effect of global dust processes on various aspects of Earth's ecosystem is discussed in reviews [63–69]. The process of saltation can be roughly separated into four stages [29, 68]: (1) The excitation of saltation: bouncing of particles under the action of an aerodynamic force; (2) ballistic motion of particles; (3) impact on the surface of particles falling under the action of gravity; (4) modification of the vertical wind profile by jumping particles. On impact, particle adhesion is reduced, and smaller particles are blown from the surface. Collisions among small saltating particles can also put larger particles into motion. However, acceleration of particles $\sim$ 500 μm in diameter is very limited due to their large inertia, and therefore they do not participate in saltation. When saltating particles interact with whirlwinds [67–71], small dust particles are raised from the surface. Vertical whirlwinds with a reduced pressure at their center lift sand and dust from the surface, carrying them to an altitude of several kilometers. Small-scale dust with particles less than 20 μm in diameter can stay in the atmosphere for up to several weeks, carried by zonal winds over distances of several thousand kilometers from their source, thus influencing the weather and climate in large regions.

2.5 Dust electrification

Hot particles of dust and sand blown by wind in a dry atmosphere acquire an electric charge on numerous collisions as a result of the triboelectric effect, which consists of the accumulation of charge upon colliding. Colliding heavy particles (of larger size) lose their electrons, which are transferred to lighter particles [9, 72]. In the presence of gravity, lighter particles are carried upward, leaving heavier particles beneath and creating vertical charge stratification and generating an electric field in a whirlwind. The generation of an electric field has been observed in vortices and also explored in laboratory modeling experiments [73–79]. Pioneering measurements by Schmidt et al. [80] showed that in terrestrial conditions, electric fields exceeding 160 kV m^{-1} can be created in dust updrafts for moderate winds. Strong electric fields in excess of 100 kV m^{-1} have been observed during dust storms and in DDs [20, 75, 81–83]. Field measurements [84] during sand storms and DDs in the western Sahara indicated that variations in the electric field can be stronger than was assumed earlier. The charge density occurring in DDs can reach values of $10^5 - 10^7$ electrons per m^3. The vortical motion of charges creates a weak magnetic field, of the order of several nanotesla. At present, considerable attention is dedicated to exploring electric fields in DDs (see, e.g., [85–89]).

In the Martian atmosphere, electric fields generated in DDs can reach values of 5–20 kV m^{-1}, corresponding to electrical breakdown. Micro-discharges occurring in such fields can generate broadband electromagnetic radiation with wavelengths in the range 1.3–6.0 cm. The role of hydrodynamic and electromagnetic forces in the formation of DDs was explored by NASA in the framework of the MATADOR project (Martian ATmosphere And Dust in the Optical and Radio) [90–91], as well as in laboratory studies and numerical modeling [92–94]. These studies indicated that the action of an electric field on the dynamics of processes and trajectories of dust particles can be ignored in the first approximation because of its smallness relative the hydrodynamic effects [90]. The triboelectric effect, underlying charge separation in a gravity field, passed tests for being used in industrial applications, in particular in pharmaceutical industry for the separation of dust (powder) particles according to mass and size in vortical motion [95–99].

3. Dust devils on Earth and Mars: main physical parameters

3.1 Dust devils on Earth

DDs are most frequently encountered in arid and desert regions on Earth: in Africa [18, 74, 100, 101], Australia [31, 102], southwest states of the USA [10, 11, 20, 25, 26, 28–30, 38, 103–108], and other regions. The results of statistical

studies of DD spatial scales are presented in Refs [14, 25, 26, 29, 36, 105]. The height of a DD depends on atmospheric conditions and dust composition, and their visible height also depends on how much dust is entrained by the vortex. The height of most DDs is at least five times larger than their diameter [31]. Most DDs are from 1 to 15 m in diameter and from several meters to one kilometer, or even more, in height [101]. According to review [9], 50% of DDs are 3–50 m high. The most powerful DDs on our planet occur in Australia, 30–140 m in radius and up to 4500 m in height. The DD life span increases with their spatial scale. It is usually from several seconds to 20 min, with most DDs lasting 1–4 min [13, 17, 109].

There is proof that the generation of a DD bears a pulsating character, with intermittent quiescent periods [14, 105]. Carroll and Ryan [38] mention that characteristic quiescent periods last 5–15 min and interpret their duration in terms of the characteristic time of convective instability. Commonly, DDs propagate at the speed of the ambient wind [100]. Their rotation speed typically equals 5–10 m s^{-1}, and does not exceed 25 m s^{-1}, and the vertical velocity does not exceed 10 m s^{-1} [9]. The observations by Sinclair [14] enabled him to formulate ideal conditions for DD generation: (1) an abundance of a loose dusty surface; (2) 'hot spots', or areas with anomalously high soil temperature; (3) local obstacles to winds, which cause the ambient vorticity of the flow. Sinclair [13] roughly split a typical structure of DDs into a lower part in the form of a 'skirt', a central part in the form of a vertical column of rapidly rotating dust, and an upper part where rotation decays and vertical flow decreases. The lowest part of the vortex — the 'skirt' — is loaded with heavier particles [17, 100]. The rotation velocity in such vortices attains a maximum at the characteristic radius of the DD and tends to zero at the periphery. The behavior of the observed velocity agrees with the behavior of rotation velocity in a stationary Rankine vortex [9, 13, 28, 109]. In such a vortex, loaded with dust, the dust flow from the inner and outer vortex regions is directed to the region where the rotation velocity is maximal.

The photo in Fig. 1 shows the 'skirt', and higher, in the inner part of the vortex, an axisymmetric domain with a reduced dust concentration [110, 111]. Heavier and larger dust particles are confined close to the ground, forming a dust cloud in the 'skirt', whereas lighter particles are transported into the upper part of the vortex. It can also be seen that in the upper part of the DD, dust particles are concentrated at the vortex boundary, where the rotation velocity is maximal.

According to laboratory studies [67, 112], the rate (flux) of dust transport equals $1.0 \times 10^{-5} - 3.0 \times 10^{-2}$ kg $m^{-2}\,s^{-1}$, which agrees well with the results of field observations [9, 32]: $0.6 \times 10^{-3} - 3.0 \times 10^{-3}$ kg m^{-2} s^{-1} [9, 32]. DDs play an important role in the transport of dust in the atmosphere [44, 45, 48, 55, 113, 114], lifting several kilograms of dust every 20 min. DDs affect soil erosion, transporting dust from the planet surface, and modify surface albedo. The height of a DD can be determined remotely from the ground or airplanes, and the observations of 'thermals' over large DDs were carried out from gliders. At altitudes of 2000–4000 m, warm updrafts were observed, with the temperature exceeding the ambient temperature by several tenths of a degree and vertical velocities of 2–4 m s^{-1} over areas of 1–5 km^2. This implies that dust particles were related to broader updrafts of rising warm air reaching several kilometers in height and expanding to several kilometers in diameter before returning down [115]. Fine African dust can be carried to southern Europe [101] and each summer reaches the Caribbean basin and southwest USA [54, 55, 59] with the concentration in the range 10–100 mg m^{-3}. This makes from one third to one half of the mass of observed dust particles with a diameter smaller than 2.5 μm.

Figure 1. Dust devil with a 'skirt' saturated with dust and an axisymmetric domain above with a reduced concentration of dust inside the vortex. The photo is from the collection *Inflow Images* (John Roenfeldt and Ira Fehlberg).

According to Refs [74, 116–120], the electric field in terrestrial DDs with a diameter of about 10 m and height of 100–200 m can reach several hundred kV m^{-1}. The corresponding charge density can reach $10^5 - 10^7$ electrons per m^3. The vortical motion of charges generates a weak magnetic field of the order of several nanoteslas.

3.2 Dust devils on Mars

DDs and possibly related dust storms are one of the most interesting atmospheric phenomena on Mars. The existence of DDs on Mars was predicted in Refs [121–124] even before their discovery. DDs on Mars were first observed in the 1970s in the framework of the NASA Viking space program [125]. These structures were initially observed as small bright clouds with long shadows [41]. The first sharp image of a Martian DD was obtained during the NASA Pathfinder mission [32, 126] in 1997.

Later, when observations with high-resolution cameras aboard the Mars Observer and Mars Surveyor missions became available, a large number of DDs were identified [11, 127, 128]. The processes of DD occurrence on Mars and Earth are similar: the ground is heated through insolation during the day time, warming the adjacent air layers. In the

Martian atmosphere, characterized by low heat capacity, turbulent and radiation fluxes can differ substantially from those in the atmospheric surface layer [129, 130]. Because of the rarefied atmosphere and weaker gravity field, DDs on Mars are much more powerful: they are much wider (sometimes by almost 50 times) and taller (by several dozen times) than their terrestrial counterparts. For example, the Mars Reconnaissance Orbiter, with the help of the HiRISE (High Resolution Imaging Experiment) camera, recorded a giant DD 20 km in height, rushing over the Martian expanses; in spite of the considerable height of the dust column, its diameter was only 64 m. Usually, Martian DDs have a diameter from 100 m to 1 km and a height up to 7–8 km.

A typical feature of Martian DDs is the appearance of several vortices simultaneously. For example, in May 2005, Mars Rover Spirit simultaneously registered three DDs traveling close to each other. In the region of the Gusev Crater, 5 to 7 DDs were seen simultaneously at noon time. In this region, DDs with a diameter of 1–2 km and height of 8–10 km were observed from the Viking orbiter.

Mars is often dominated by dust storms: winds unceasingly grind the upper dried-up dust layer, and haze covers extensive areas of the planet. In such periods, DDs appear so frequently that numerous tracks mutually intersect, leaving marks of DD trajectories on the ground. Intricate footprints left on the Martian surface by large dust whirlwinds were discovered in many regions of the red planet, and images of several DDs were taken when they were 'moulding' the surface in this way. Dark traces are formed as vortices pass, lifting dust and revealing bedrock.

To estimate the wind velocities, which are needed to refine climate models, the studies of DD propagation velocities were carried out. Assuming that Martian DDs move with the wind velocity, just like their terrestrial counterparts, their measured velocity can serve as an estimate of wind velocities on Mars. From orbital observations by the ESA (European Space Agency) Mars Express High Resolution Stereo Camera, it follows that DDs travel over the Martian surface with velocities of the order of several dozen meters per second. Wind and DDs related to it may influence the mechanisms initiating giant dust storms. According to estimates [67, 112, 131, 132], Martian DDs annually lift 2×10^{11} kg of dust into the atmosphere, which has a noticeable impact on the climate of the planet. Studies in the MATADOR project were dedicated to the effect of hydrodynamic and electromagnetic forces on DD formation [117–120]. Analogous laboratory studies were also carried out [86, 92, 93, 133]. As follows from these studies, the effect of an electric field on the dynamics of processes and trajectories of dust particles can be disregarded in the first approximation because of its smallness compared to the effect of hydrodynamic flows [119].

Electric fields created in DDs are governed by vertical currents of charged particles and the distribution of velocity as a function of mass. As a result of these processes, the electric field grows exponentially with time and can reach values that correspond to electrical breakdown in the Martian conditions [134, 135]. Micro-discharges developing in such fields can generate broadband electromagnetic radiation.

4. Analytic models of stationary vortices

Despite the relevance of studying CVs such as tornados and DDv, their theoretical analysis is still far from the role it could play in predicting the dynamics of such vortex structures. The internal structure, strength, and scale of a vortex to a large degree determine the stability of the vortex and the way it interacts with other vortices and the ambient flow.

At present, only a small number of exact solutions of the Navier–Stokes equations describing the structure of stationary vortices is known. We mention Burgers (or Burgers–Rott) vortices [136, 137] and Sullivan vortices [138]. Because these solutions suffer from a number of drawbacks, searching for new exact solutions of fluid dynamics equations describing vortical fluid motions is a compelling task. It is hoped that its solution will open up the simplest and most rigorous way of obtaining a number of theoretically and practically important results.

In contrast to vortices of a planetary scale (vortices of Rossby waves, cyclones, or anticyclones; see, e.g., [139], [140]), CVs are small-scale structures. In exploring such structures in planetary atmospheres, we can ignore the Coriolis force. Furthermore, in considering flows with velocities much smaller than the speed of sound, we ignore compressibility. In Section 4.1, we present the full system of Navier–Stokes equations for an incompressible fluid as a system of equations governing the fluid dynamics. In Sections 4.2–4.4, we discuss the simplest models of vortices used to interpret observations: the models by Rankine, Burgers, and Sullivan. In Section 4.5, we present a model of concentrated vortices that are exponentially localized in space, allowing a description of the main features of their structure.

4.1 Main basic equations

As a basic set of fluid dynamics equations, we take the Navier–Stokes equation

$$\frac{\mathrm{d}\mathbf{v}}{\mathrm{d}t} = -\frac{1}{\rho}\,\nabla p + \mathbf{g} + \nu\Delta\mathbf{v} \tag{1}$$

and the incompressibility condition

$$\nabla\,\mathbf{v} = 0\,. \tag{2}$$

Here, $\mathrm{d}/\mathrm{d}t = \partial/\partial t + \mathbf{v}\nabla$ is the convective (full) time derivative, $\mathbf{v}$ is the velocity, ρ and p are the density and pressure, ν is the kinematic viscosity, and $\mathbf{g} = -g\hat{\mathbf{e}}_z$ is the acceleration of gravity, with $\hat{\mathbf{e}}_z$ a unit vector directed along the vertical z axis. Here, we explore stationary structures, assuming $\partial/\partial t = 0$.

To describe the simplest vortical motion in stationary structures, we make the approximation of axial symmetry, $\partial/\partial\varphi = 0$. In a cylindrical coordinate system (r, ϕ, z), system of equations (1) and (2) takes the form

$$v_r\frac{\partial v_r}{\partial r} + v_z\frac{\partial v_r}{\partial z} - \frac{v_\phi^2}{r} + \frac{1}{\rho}\frac{\partial p}{\partial r} = \nu\left(\frac{\partial^2 v_r}{\partial r^2} + \frac{1}{r}\frac{\partial v_r}{\partial r} - \frac{v_r}{r^2}\right), \tag{3}$$

$$v_r\left[\frac{1}{r}\frac{\partial}{\partial r}\,rv_\phi\right] + v_z\frac{\partial v_\phi}{\partial z} = \nu\left(\frac{\partial^2 v_\phi}{\partial r^2} + \frac{1}{r}\frac{\partial v_\phi}{\partial r} - \frac{v_\phi}{r^2}\right), \tag{4}$$

$$v_r\frac{\partial v_z}{\partial r} + v_z\frac{\partial v_z}{\partial z} + \frac{1}{\rho}\frac{\partial p}{\partial z} = \nu\left(\frac{\partial^2 v_z}{\partial r^2} + \frac{1}{r}\frac{\partial v_z}{\partial r} + \frac{\partial^2 v_z}{\partial z^2}\right), \tag{5}$$

$$\frac{\partial v_r}{\partial r} + \frac{v_r}{r} + \frac{\partial v_z}{\partial z} = 0\,. \tag{6}$$

Usually, most of the time the atmosphere is in equilibrium that is close to hydrostatic equilibrium with the gravitational

attraction balanced by the pressure gradient. In this state, $p = p_0 \exp(-z/H)$, where $H = p_0/(\rho g)$ is the height of the equilibrium atmosphere. Structures with a characteristic height that is much smaller than H are discussed below.

4.2 Rankine vortex

The Rankine vortex model [15] is frequently invoked to interpret observations and the results of laboratory and numerical modeling. Observational data on DDs, as well as results of numerical modeling [8, 9, 26, 28, 141–145], agree satisfactorily with the Rankine vortex model. This model describes stationary planar vortical motion with zero vertical and radial velocities, $v_r = v_z = 0$. The azimuthal velocity is written as

$$v_\phi = \frac{a}{r} + br\,, \tag{7}$$

where the constants a and b are determined from the boundary conditions. Equation (1) leads to the cyclostrophic equilibrium condition

$$p = \rho \int_0^r \frac{v_\phi^2}{r}\,\mathrm{d}r\,. \tag{8}$$

The Rankine vortex corresponds to a piecewise-continuous solution of Navier–Stokes equations. The condition $a = 0$ for $r < r_0$ corresponds to a solid-body rotation inside the vortex, and the condition $b = 0$ corresponds to a potential flow in the outer domain. The azimuthal velocity attains its maximum at the radial distance $r = r_0$. The Rankine vortex is called a combined vortex because it consists of two domains (the inner and outer) with a distinct motion character. We note that the velocity profile in the stationary Rankine vortex agrees well with observations of DDs, whose rotation velocity reaches a maximum at a characteristic radius and tends to zero at the periphery. A modification of the Rankine vortex in the approximation when the characteristic vortex radius r_0 is a function of the coordinate z was explored in Refs [23, 35–37].

Although this model with a piecewise continuous azimuthal velocity is not an exact solution of Navier–Stokes equations and hence is not fully applicable to studying motions in the atmosphere, it is nevertheless frequently used to interpret observations and the results of numerical simulations of CV dynamics,

4.3 Burgers vortex

One of the exact solutions of the Navier–Stokes equations for three-dimensional stationary incompressible motions of viscous fluid is the Burgers (or Burgers–Rott) vortex [136, 137]. In the axially symmetric Burgers vortex, all three components of velocity differ from zero. The radial component of velocity in the vortex is directed to the center, the vertical one is proportional to z and directed upward, and the azimuthal velocity is an arbitrary function of the radius,

$$v_r = -\frac{\alpha}{2}\,r\,, \quad v_\phi = v_\phi(r)\,, \quad v_z = \alpha z\,, \tag{9}$$

where $\alpha > 0$ is a constant governing the suction of fluid in the vortex. Because the azimuthal velocity depends only on the radial distance and the vertical one increases linearly with height, it follows from equation (4) that

$$v_r\left(\frac{1}{r}\frac{\partial}{\partial r}\,rv_\phi\right) = \nu\left(\frac{\partial^2 v_\phi}{\partial r^2} + \frac{1}{r}\frac{\partial v_\phi}{\partial r} - \frac{v_\phi}{r^2}\right). \tag{10}$$

The left-hand side of Eqn (10) corresponds to a nonlinear effect of vertical vorticity amplification under radial compression of vortex tubes, whereas the right-hand side describes viscous diffusion of vorticity acting against the amplification. In a reference frame moving together with the flow, the solution of Eqn (10) exists if both effects equilibrate each other. In this case, the azimuthal velocity is expressed as

$$v_\phi = \frac{\Gamma}{2\pi r}\left[1 - \exp\left(-\frac{r^2}{2R_\mathrm{B}^2}\right)\right], \tag{11}$$

where $R_\mathrm{B} = 2\nu/\alpha$ is the characteristic radius of the Burgers vortex and Γ is the circulation:

$$\Gamma = 2\pi \int_0^\infty \omega_z r\,\mathrm{d}r\,. \tag{12}$$

The azimuthal velocity attains a maximum at the radial distance $r = 1.12R_\mathrm{B}$. Inside the vortex, where $r \ll R_\mathrm{B}$, and far away at its periphery, where $r \gg R_\mathrm{B}$, the radial dependences of the azimuthal velocity in the Rankine and Burgers vortices behave similarly. The Burgers vortex has only one nonzero vorticity component $\boldsymbol{\omega} = (0, 0, \omega_z)$, where

$$\omega_z = \frac{\Gamma}{4\pi\nu}\exp\left(-\frac{r^2}{2R_\mathrm{B}^2}\right). \tag{13}$$

The pressure in the vortex takes the form

$$p = p_0 - \frac{\rho\alpha^2}{8}\,(r^2 + 4z^2) + \rho\int_0^r \frac{v_\phi^2}{r}\,\mathrm{d}r\,. \tag{14}$$

Just as in the Rankine vortex, the fluid rotates around the z axis; however, in the Burgers vortex, in addition to the finite azimuthal velocity, the poloidal (radial and vertical) velocity components also differ from zero. In such a vortex, the fluid follows a spiral, approaching the center of rotation and accelerating upward. In concentrated vortices such as DDs or typhoons, in addition to rotation around some vertical axis, there is also suction of fluid into the vortex and its upward transport. For this reason, the Burgers vortex model proves to be more relevant than the Rankine vortex for interpreting atmospheric vortices. The radial and vertical velocity components are proportional to the parameter α characterizing the fluid suction into the vortex. The Burgers vortex and its nonstationary modifications are discussed in [146] from the standpoint of constructing models of evolving vertical vortices.

Even though the Burgers model offers some advantages over the Rankine model, it also has a number of drawbacks. In the Burgers model, the radial and vertical velocities increase without bounds with the distance from the vortex center and the planet surface, respectively. For this reason, the Burgers model is inapplicable for large heights and radial distances. However, for moderate heights and radial distances within two or three vortex radii, this model can be used to interpret observations and numerical modeling results.

4.4 Sullivan vortex

The Sullivan vortex [138], just like the Burgers vortex, is an exact solution of the Navier–Stokes equations. In this vortex, just as in the Burgers vortex, all three velocity components

differ from zero:

$$v_r = -\frac{\alpha}{2}\, r + \frac{6\nu}{r}\left[1 - \exp\left(-\frac{\alpha r^2}{4\nu}\right)\right],\ v_\phi = \frac{\Gamma H(\alpha r^2/4\nu)}{2\pi r H(\infty)},$$
$$v_z = \alpha z\left[1 - 3\exp\left(-\frac{\alpha r^2}{4\nu}\right)\right], \tag{15}$$

where

$$H(x) = \int_0^x \exp\big(f(t)\big)\,\mathrm{d}t,\ f(t) = -t + 3\int_0^t \frac{1-\exp(y)}{y}\,\mathrm{d}y. \tag{16}$$

The azimuthal and vertical vorticity components take the form

$$\omega_\phi = -\frac{\alpha^2 rz}{\nu}\exp\left(-\frac{\alpha r^2}{2\nu}\right), \tag{17}$$

$$\omega_z = \frac{\Gamma\alpha}{2\pi\nu H(\infty)}\exp\big(f(r)\big). \tag{18}$$

The pressure in such a vortex is expressed as

$$p = p_0 - \frac{\rho\alpha^2}{8}\,(r^2 + 4z^2) + \rho\int_0^r \frac{v_\phi^2}{r}\,\mathrm{d}r - \frac{18\rho\nu^2}{r^2}\left[1 - \exp\left(-\frac{\alpha r^2}{4\nu}\right)\right]^2. \tag{19}$$

In contrast to the Burgers vortex, the Sullivan vortex has a two-cell structure. In the central vortex part (central cell), the vertical velocity is directed downward, and the radial velocity is directed outside. In the outer vortex region (outer cell), the vertical velocity is upward, and the radial one is directed to the center of the vortex. The Sullivan vortex is the simplest two-cell dissipative vortex, which is used to interpret strong DDs and to describe tornado vortices [3, 7, 147]. Just as in the Burgers vortex, its vertical and radial velocities increase without bounds with, respectively, height and radial distance.

Admittedly, a tornado is too complex a phenomenon to be fully described in the framework of a simple stationary hydrodynamic model. However, the exact solution of the Navier–Stokes equations contains important information on the structure of possible vortical flows. A central point in the formation of dissipative stationary Burgers and Sullivan vortices is the balance between the effects of vorticity amplification in the flow toward the vortex center and vorticity decay owing to viscous diffusion. This leads to the question of whether stationary CVs are possible in a medium without dissipation.

4.5 Model of concentrated dissipation-free vortices

The Burgers and Sullivan vortices are called dissipative because viscosity plays a key role in them. If viscosity is decreased, the vortices spread in space, decay, and finally disappear. The right-hand side of Eqn (4) describing the dynamics of vertical vorticity in an inviscid medium is identically equal to zero. However, we note that the second term in the left-hand side of this equation can be, generally speaking, different from zero if the azimuthal velocity depends not only on the radius but also on the height. A simple model of a stationary CV in an ideal incompressible fluid was studied in Ref. [148]. In this model, just as in the Burgers and Sullivan models, the vortex is localized in the radial direction, but is not localized vertically. For this reason, this model is applicable only to small altitudes, comparable to the vortex radius. This model was further developed to interpret vortices localized not only over radius but also vertically in Refs [51, 149, 150].

We begin with the Euler equations

$$v_r\frac{\partial v_r}{\partial r} + v_z\frac{\partial v_r}{\partial z} - \frac{v_\phi^2}{r} = -\frac{1}{\rho}\frac{\partial p}{\partial r}, \tag{20}$$

$$v_r\left(\frac{1}{r}\frac{\partial}{\partial r}\,rv_\phi\right) + v_z\frac{\partial v_\phi}{\partial z} = 0, \tag{21}$$

$$v_r\frac{\partial v_z}{\partial r} + v_z\frac{\partial v_z}{\partial z} = -\frac{1}{\rho}\frac{\partial p}{\partial z} \tag{22}$$

and continuity equation (6). The velocity of incompressible fluid in an axially symmetric flow can be split into the poloidal velocity $\mathbf{v}_\mathrm{p} = (v_r, 0, v_z)$ and the azimuthal velocity $v_\phi\hat{\mathbf{e}}_\phi$. Here, $\mathbf{e}_\phi$ is the unit vector along the corresponding coordinate axis. The poloidal velocity is expressed in terms of the streamfunction ψ as $\mathbf{v}_\mathrm{p} = \nabla\times(\psi\nabla\phi)$. Accordingly, the radial and vertical velocity components are expressed through the streamfunction as

$$v_r = -\frac{1}{r}\frac{\partial\psi}{\partial z}, \qquad v_z = \frac{1}{r}\frac{\partial\psi}{\partial r}. \tag{23}$$

Equation (21) can be transformed into the angular momentum conservation equation for a unit mass, $M = rv_\phi$,

$$v_r\frac{\partial M}{\partial r} + v_z\frac{\partial M}{\partial z} = 0. \tag{24}$$

The first term in Eqn (24) describes the angular momentum amplification in a flow converging to the center, and the second term describes its attenuation due to vertical transport. Using relations (23) that express the poloidal velocity components through the streamfunction, we can rewrite Eqn (24) as

$$J\{\psi, M\} = 0, \tag{25}$$

where $J\{a,b\} = (\partial a/\partial r)\,\partial b/\partial z - (\partial a/\partial z)\,\partial b/\partial r$ is the Jacobian. A solution of (25) is given by $M = f(\psi)$, where $f(x)$ is an arbitrary function. As a particular solution of Eqn (25), we use the relation $M = A\psi$, where A is some dimensional constant. Hence follows the expression for the azimuthal velocity

$$v_\phi = \frac{A\psi}{r}. \tag{26}$$

Thus, all velocity components are expressed in terms of the streamfunction ψ with the help of Eqns (23) and (26). To complete the solution, it remains to derive an equation for the pressure p. To relate the pressure to the streamfunction, we use the known identity $(\mathbf{v}\nabla)\,\mathbf{v} = \nabla(v^2/2) - \mathbf{v}\times(\nabla\times\mathbf{v})$ to transform (20) and (22) into the equation

$$\frac{\partial}{\partial r}\left(p + \rho\frac{v_r^2}{2} + \rho\frac{v_z^2}{2}\right) - \rho v_z\omega_\phi - \rho\frac{v_\phi^2}{r} = 0, \tag{27}$$

$$\frac{\partial}{\partial z}\left(p + \rho\frac{v_r^2}{2} + \rho\frac{v_z^2}{2}\right) + \rho v_r\omega_\phi = -\rho g. \tag{28}$$

Because the vertical scale L of vortex structures is commonly much smaller than the equivalent height of the atmosphere $H = p_0/(\rho g)$, $L \ll H$, we have $p = p_0$. In the approximation of incompressible fluid used here, we assume that the pressure perturbation δp is small compared to the equilibrium atmospheric pressure p_0. In the approximation of thin vortex tubes adopted here, $r_0 \ll L$, from Eqns (27) and (28) we obtain a simplified equation for the pressure:

$$p = p_0 - \rho\frac{v_z^2}{2} + \rho\int_0^r \frac{v_\phi^2}{r}\,\mathrm{d}r\,. \tag{29}$$

Equations (23), (26), and (29) relate all hydrodynamic fields to the streamfunction. When choosing a concrete form for $\psi(r,z)$, we rely on the following conditions for the velocity components v_r, v_z, v_ϕ and pressure p:

(a) $v_r = v_\phi = 0$, and v_z and p are finite on the vortex axis at $r = 0$;

(b) $v_z = v_\phi = 0$, and v_r and p are finite on the underlying surface at $z = 0$;

(c) $v_r = v_z = v_\phi = 0$ and $p = p_0$ at the vortex periphery at $r/r_0 \gg 1$ and $z/L \gg 1$, where r_0 and L are characteristic spatial scales of the vortex in the radial and vertical directions.

Given conditions (a)–(c), we select the streamfunction in the form

$$\psi = v_0 r^2\,\frac{z}{L}\exp\left(-\frac{z}{L}-\frac{r^2}{r_0^2}\right), \tag{30}$$

where v_0 is the characteristic poloidal velocity. Using Eqns (23), (26), and (29), we then obtain

$$\frac{v_r}{v_0} = -\frac{r}{L}\left(1-\frac{z}{L}\right)\exp\left(-\frac{z}{L}-\frac{r^2}{r_0^2}\right), \tag{31}$$

$$\frac{v_z}{v_0} = 2\frac{z}{L}\left(1-\frac{r^2}{r_0^2}\right)\exp\left(-\frac{z}{L}-\frac{r^2}{r_0^2}\right), \tag{32}$$

$$\frac{v_\phi}{v_{\phi 0}} = \frac{r}{r_0}\,\frac{z}{L}\exp\left(-\frac{z}{L}-\frac{r^2}{r_0^2}\right), \tag{33}$$

where v_0 is the characteristic azimuthal velocity. Taking Eqns (32) and (33) into account, we reduce Eqn (29) for pressure to the form

$$\frac{p-p_0}{\rho v_0^2} = \frac{1}{4}\left(\frac{z}{L}\right)^2\exp\left(-2\frac{z}{L}\right)\left\{\frac{v_{\phi 0}^2}{v_0^2}\left[1-\exp\left(-2\frac{r^2}{r_0^2}\right)\right] - 8\left(1-\frac{r^2}{r_0^2}\right)^2\exp\left(-2\frac{r^2}{r_0^2}\right)\right\}. \tag{34}$$

Equations (31)–(33) for velocity components together with Eqn (34) for pressure correspond to an exact analytic solution of Euler equations (20)–(22).

Using Eqn (33) for the azimuthal velocity, we can obtain the following expression for the vertical vorticity:

$$\omega_z = \frac{1}{r}\frac{\partial}{\partial r}rv_\phi = \omega_{z0}\frac{z}{L}\left(1-\frac{r^2}{r_0^2}\right)\exp\left(-\frac{z}{L}-\frac{r^2}{r_0^2}\right), \tag{35}$$

where $\omega_{z0} = 2v_{\phi 0}/r_0$. In contrast to the Rankine and Burgers vortices, the structure explored here also has a finite horizontal vorticity

$$\omega_\phi = (\nabla\times\mathbf{v})_\phi = -4\,\frac{v_0}{r_0}\,\frac{rz}{r_0 L}\left(2-\frac{r^2}{r_0^2}\right)\exp\left(-\frac{z}{L}-\frac{r^2}{r_0^2}\right). \tag{36}$$

The new model, just like the Burgers and Sullivan models, is applicable if friction can be ignored in the surface layer (see, e.g., [151, 152]). We note that the applicability of the new model is limited by the condition $z \gg r$, which is valid in the interval of finite heights $z > r_0$, where friction can be ignored.

It follows from Eqns (32), (35), and (36) that the vertical velocity and vertical and horizontal vorticities change sign at the boundary or close to the jet boundary. From Eqns (31)–(36), it also follows that all hydrodynamic fields, including vorticities, are exponentially localized vertically as well as radially.

Our model allows calculating the vertical and radial mass fluxes. The vertical mass flux $M_z = 2\pi\rho\int_0^\infty v_z r\,\mathrm{d}r$ consists of an upward flux in the inner vortex part,

$$M_{1z} = 2\pi\rho\int_0^{r_0} v_z r\,\mathrm{d}r = 2\pi r_0^2\rho v_0\,\frac{z}{L}\exp\left(-1-\frac{z}{L}\right), \tag{37}$$

and a downward flux in the vortex tail,

$$M_{2z} = 2\pi\rho\int_{r_0}^\infty v_z r\,\mathrm{d}r = -2\pi r_0^2\rho v_0\,\frac{z}{L}\exp\left(-1-\frac{z}{L}\right), \tag{38}$$

which compensate each other. The radial mass flux $M_r = 2\pi\rho r\int_0^\infty v_r\,\mathrm{d}z$ also consists of two oppositely directed fluxes: the flux directed toward the vortex axis in the lower part of the vortex,

$$M_{1r} = 2\pi\rho r\int_0^L v_r\,\mathrm{d}z = -2\pi\rho v_0 r^2\exp\left(-1-\frac{r^2}{r_0^2}\right), \tag{39}$$

and the opposite flux in the upper part,

$$M_{2r} = 2\pi\rho r\int_L^\infty v_r\,\mathrm{d}z = 2\pi\rho v_0 r^2\exp\left(-1-\frac{r^2}{r_0^2}\right). \tag{40}$$

Hence, it follows that in our model, where the vertical and horizontal mass fluxes equal zero, $M_z = 0$ and $M_r = 0$, the mass is conserved. In Burgers and Sullivan vortices, vertical and radial mass fluxes grow without bounds if the height z or the radius are increased, which limits their applicability for interpreting the observed CVs.

In the new model, the vortical flow is exponentially localized not only radially but also vertically with a characteristic scale L. The structure of the vortex in the vertical direction can be roughly split into three domains: the foundation (skirt) and the central and upper parts. In the radial direction, we can distinguish the inner and outer vortex parts, for $r < r_0$ and $r > r_0$, respectively. In the skirt, for $z \ll L$, the vertical and azimuthal components of velocity are small. They increase in the inner part with an increase in height. At the height $z = L$, the vertical and azimuthal velocities and the vertical vorticity attain maximum values. In the upper part of the vortex, the ascending motion and motion directed to the center are transformed into a descending and radially spreading flow. Such a model describes all the main characteristics of DDs in the quasi-stationary stage.

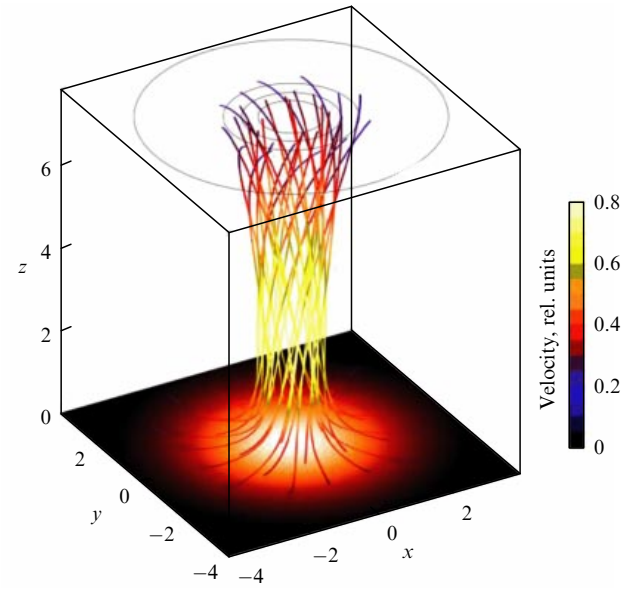

Figure 2. (Color online.) Three-dimensional trajectories of particles and velocities of vortical motion.

Three-dimensional trajectories of particles and their velocities in vortical motion are depicted in Fig. 2, which shows a vortex with the ratio of characteristic velocities (azimuthal to poloidal) $v_{\phi 0}/v_0 = 5$. In dimensionless units, the vortex radius is $r_0 = 2$, and the characteristic vertical scale of the vortex is $L = 2.75$. The particles shown in Fig. 2 were initially at the radial distance $r = r_0$.

Figure 3 shows the distribution of the dimensionless pressure $\bar{p} = (p - p_0)/(\rho v_0^2)$ in the vortex in the radial direction at different heights. The following values of parameters were taken: $v_{\phi 0}/v_0 = 4$, $r_0 = 2$, and $L = 2.75$. Radial pressure distributions are shown at heights $z/L = 0.64$; 0.95; 1.28; 1.60; 1.92; 2.24; 2.56; and 2.88.

The trough in the pressure distribution comes from poloidal motion in the vortex. The negative pressure in the trough describes the effect of fluid suction in the central vortex region. The pressure crest in the central vortex part is due to the action of the centrifugal force. With an increase in height in the upper vortex part, the poloidal motion and azimuthal velocity weaken, and the trough and crest decrease in pressure accordingly.

5. Generation of concentrated vortices in an unstably stratified atmosphere

According to current views, one of the main mechanisms of DD generation is anomalous heating of the planet surface by insolation. The heating of soil is accompanied by a superadiabatic temperature gradient and an ascending convective flow of warm air. Meteorological observations [25, 28] laid the basis for constructing the first thermodynamic model of DD generation [34, 153, 154]. According to this model, warm air in a convectively unstable atmosphere moves upward and, after being cooled, descends. Such a model is an analog of the thermal engine taking energy from the warm surface layer. The model in [34] predicts that the intensity of a DD depends on the product of vertical and horizontal temperature gradients.

Sinclair [14], based on long-term observations of DDs, proposed that the necessary condition for the occurrence of a DD is the presence of dust and sites where the soil temperature is anomalously high in the atmospheric surface layer. According to current views [9, 35, 145, 155–157], DDs are formed from convective cells (jets). Convective cells form in an unstable surface layer with a superadiabatic temperature gradient. Observations showed that the generation of vortices rotating clockwise (anticyclonic) and counterclockwise (cyclonic) is equally probable on open terrain. From the observed absence of correlation between the external vorticity, the generation time, and the vortex diameter, it follows that the presence of only some ambient vorticity in the atmosphere is insufficient for DD generation. In Section 5.2,

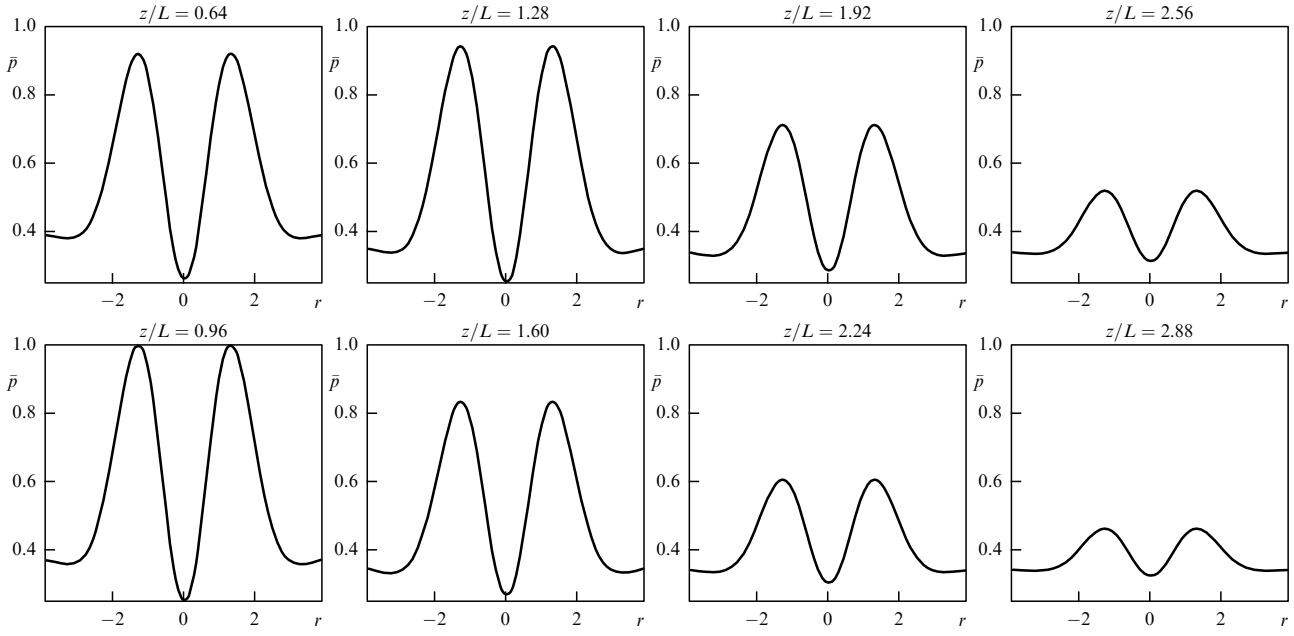

Figure 3. Radial distribution of the dimensionless pressure $\bar{p}$ in the vortex at different heights z/L. It is assumed that $v_{\phi 0}/v_0 = 4$, $r_0 = 2$, and $L = 2.75$.

we discuss the generation of updrafts in the surface atmospheric layer with a superadiabatic temperature gradient. As indicated by DD observations, at the stage of updraft generation, a rapid amplification of azimuthal velocity is observed, which is responsible for the fast transformation of updrafts into vortices. This phenomenon is discussed in Section 5.3.

5.1 Simplified equations for nonlinear internal gravity waves

According to current views, one of the most important channels connecting the lithosphere and the atmosphere involves internal gravity waves (IGWs). The frequency of IGWs lies in the range $|\omega_g| \geqslant |\omega| \gg |f|$, where $f = 2\Omega \sin\varphi$ is the Coriolis parameter, Ω is Earth's rotation frequency, and φ is the latitude. We start from the fluid motion equation

$$\rho \frac{d\mathbf{v}}{dt} + \nabla p - \rho \mathbf{g} = 0 \tag{41}$$

and the transport equation for the potential temperature $\Theta = p^{1/\gamma_a}/\rho$, which is a single-valued function of entropy,

$$\frac{d\Theta}{dt} = 0 . \tag{42}$$

Here, as in Section 4, ρ and p are the density and pressure, $d/dt = \partial/\partial t + \mathbf{v}\nabla$ is the material (convective) time derivative, $\mathbf{v}$ is the velocity, γ_a is the adiabatic index, $\mathbf{g} = -g\mathbf{e}_z$ is the acceleration due to gravity, and $\mathbf{e}_z$ is a unit vertical vector. The dynamics of nonlinear IGW structures in Cartesian coordinates has been studied in Refs [158–162].

As in Section 4, we study the dynamics of convective motion of axially symmetric structures in a cylindric coordinate system (r, ϕ, z), assuming $\partial/\partial\phi = 0$ and disregarding effects related to wind inhomogeneity and dissipation. As in Section 4, we express the fluid velocity as a sum of poloidal and azimuthal components, $\mathbf{v} = \mathbf{v}_p + \mathbf{v}_\phi$, where $\mathbf{v}_p = \nabla \times (\psi \nabla\phi)$ and $\mathbf{v}_\phi = v_\phi \mathbf{e}_\phi$. Here, $\mathbf{e}_\phi$ is the unit vector along the corresponding coordinate and $\psi(t, r, z)$ is the streamfunction. The radial and vertical components of the poloidal velocity are connected to the streamfunction by relations (23).

According to Refs [158, 163, 164], the following simplified equation can be used to describe the dynamics of nonlinear internal gravity waves:

$$\left(\frac{\partial^2}{\partial t^2} + \omega_g^2\right)\Delta_r^*\psi + \frac{1}{r}\frac{\partial}{\partial t} J(\psi, \Delta_r^*\psi) = 0 . \tag{43}$$

Here, ω_g is the Brunt–Väisälä frequency given by

$$\omega_g^2 = g\left(\frac{\gamma_a - 1}{\gamma_a H} + \frac{1}{T}\frac{dT}{dz}\right), \tag{44}$$

J is the Jacobian, Δ_r^* is the Grad–Shafranov operator,

$$\Delta_r^* = r\frac{\partial}{\partial r}\left(\frac{1}{r}\right)\frac{\partial}{\partial r} ,$$

T is the temperature, and $H = p/(\rho g)$ is the vertical scale of the atmosphere. In an unstably stratified atmosphere, $\omega_g^2 < 0$, and the frequency of IGWs is purely imaginary, which corresponds to their absolute instability.

5.2 Generation of vertical jets

Equation (43) is a basic one for studying the dynamics of nonlinear IGW structures in a convectively unstable atmosphere with $\omega_g^2 < 0$ [158, 163, 164]. We express the streamfunction ψ in the form

$$\psi = \frac{v_0 r^2 z}{2r_0} \exp\left(\gamma t - \frac{r^2}{r_0^2}\right), \tag{45}$$

where $v_0 > 0$ is the characteristic velocity and r_0 is the characteristic radius of the structure. Applying the Grad–Shafranov operator to this streamfunction, we obtain

$$\Delta_r^*\psi = -\frac{8}{r_0^2}\psi + \frac{4r^2}{r_0^4}\psi . \tag{46}$$

Relations (46) allows omitting the nonlinear term in Eqn (43) if

$$2\frac{v_0 r^2}{\gamma r_0^3} \exp\left(\gamma t - \frac{r^2}{r_0^2}\right) \ll 1 . \tag{47}$$

In this approximation, from Eqn (43) we obtain the expression for the increment of IGWs $\gamma = |\omega_g|$. Thus, the streamfunction given by (45) is a solution of Eqn (43) if condition (47) holds. Using relations (23), we write the poloidal velocity components as

$$v_r = -v_0 \frac{r}{r_0} \exp\left(\gamma t - \frac{r^2}{r_0^2}\right), \tag{48}$$

$$v_z = v_0 \frac{z}{r_0}\left(1 - \frac{r^2}{r_0^2}\right) \exp\left(\gamma t - \frac{r^2}{r_0^2}\right). \tag{49}$$

It follows from Eqn (48) that the radial velocity is directed to the center and does not depend on the height z. It follows from Eqn (49) that the vertical velocity is directed upward in the inner part of the jet and downward in the outer, $r > r_0$. Convective motion in the jet described by Eqns (48) and (49) has a nonzero poloidal vorticity $\omega_\phi = (\nabla \times \mathbf{v})_\phi$. Using the relations $\omega_\phi = -\partial v_z/\partial r$ connecting the toroidal vorticity with the vertical velocity, we write the toroidal vorticity as

$$\omega_\phi = 2v_0 \frac{rz}{r_0^3}\left(2 - \frac{r^2}{r_0^2}\right) \exp\left(\gamma t - \frac{r^2}{r_0^2}\right). \tag{50}$$

As can be seen from Eqns (48)–(50), the components of poloidal velocity and toroidal vorticity in the jet grow exponentially with time when the increment γ is increased. Additionally, it follows from Eqns (48)–(50) that the jet flow is exponentially localized over the radius. The toroidal vorticity, just like the vertical velocity, increases with height and changes sign in the outer vortex part.

5.3 Explosive generation of azimuthal rotation

Using expressions for the radial and vertical components of convective motion (48) and (49), we explore the generation of vortices in the atmosphere with a seed vertical vorticity $\omega_z = (\nabla \times \mathbf{v})_z$ [51, 149, 164]. The nonlinear equation describing the interaction of convective motion in the jet with the vertical vorticity takes the form

$$\frac{\partial\omega_z}{\partial t} + v_z\frac{\partial\omega_z}{\partial z} = \omega_z\frac{\partial v_z}{\partial z} - v_r\frac{\partial\omega_z}{\partial r} . \tag{51}$$

The first and the second terms in the right-hand side of Eqn (51) respectively describe convergence to the center and vertical stretching of vortex tubes. As a model for a seed large-

scale vorticity at small height $z < h$, we take $\omega_z(0,r,z) = \Omega(z/h)[1-\exp(-r^2/a^2)]$, where h is some characteristic height, and far from the surface, at $z \geqslant h$, we set $\omega_z(0,r,z) = \Omega[1-\exp(-r^2/a^2)]$. For heights $z < h$ and at a radial distance comparable to the vortex radius r_0, the initial vorticity is expressed as

$$\omega_z(0,r,z) = \Omega_{zh} \approx \Omega\left(\frac{z}{h}\right)\left(\frac{r^2}{a^2}\right), \tag{52}$$

and at a large height $z > h$,

$$\omega_z(0,r) = \Omega_z \approx \Omega\left(\frac{r^2}{a^2}\right). \tag{53}$$

Inserting expressions for the poloidal velocity components into Eqn (51), and taking the initial vorticity (52) or (53) into account, we obtain the expression for the vertical vorticity at the height $z < h$

$$\frac{\omega_z(t,r,z)}{\Omega_{zh}} = \exp\left[\frac{v_0}{\gamma r_0}\exp\left(\gamma t - \frac{r^2}{r_0^2}\right)\right], \tag{54}$$

and for $z > h$,

$$\frac{\omega_z(t,r)}{\Omega_{zh}} = \exp\left[\frac{v_0}{\gamma r_0}\left(2-\frac{r^2}{r_0^2}\right)\exp\left(\gamma t - \frac{r^2}{r_0^2}\right)\right]. \tag{55}$$

Using the relations connecting the vertical vorticity with the azimuthal velocity, $r\omega_z = \partial(rv_\varphi)/\partial r$, we find the expression for the azimuthal velocity v_φ close to the surface

$$v_\phi = v_{\phi 0h}\exp\left[\frac{v_0}{\gamma r_0}\exp\left(\gamma t - \frac{r^2}{r_0^2}\right)\right], \tag{56}$$

and at large height,

$$v_\phi = v_{\phi 0}\exp\left[2\,\frac{v_0}{\gamma r_0}\exp\left(\gamma t - \frac{r^2}{r_0^2}\right)\right], \tag{57}$$

where $v_{\phi 0h} = (\Omega a/4)(r/a)^3(z/h)$ and $v_{\phi 0} = (\Omega a/4)(r/a)^3$. It follows from Eqns (54)–(57) that the vertical vorticity and azimuthal velocity are described by a double exponential corresponding to an explosive generation.

To illustrate these results when interpreting the mechanism generating dust vortices in the terrestrial atmosphere, we take, as a characteristic value, the surface-layer temperature gradient equal to 2 °C per m [102], which is commonly observed in the surface layer when vortices are generated. Such a gradient corresponds to the convective instability increment $\gamma = 0.25\ \mathrm{s}^{-1}$.

Figure 4 displays the profiles of the three velocity components in a vortex in the range $t \leqslant 6.4$ s under the assumption $\gamma = 0.25\ \mathrm{s}^{-1}$. When computing the azimuthal velocity by formula (57), it has been assumed that $v_0 = 2\gamma r_0$. The radial and vertical velocities in Fig. 4a, b are normalized by v_0 and zv_0/r_0. For a vortex with a radius of 10 m, we find the characteristic radial velocity $v_0 = 5\ \mathrm{m\ s}^{-1}$. It can be seen that the radial velocity in Fig. 4a is always directed to the center and is negligibly small at long distances $r > 3r_0$. The velocity of the descending flow in the outer vortex part is substantially smaller than the upward velocity in the central part of the vortex. The azimuthal velocity (Fig. 4c) is normalized by $v_{\phi 0} = \Omega r_0^3/(4a^2)$. Figure 4 illustrates the velocity profiles assuming that formulas (48), (49), and (57) are valid for all radii. However, these formulas are valid in bounded intervals, for $r < r_1$ and $r > r_2$, where condition (49) holds. As time varies from $t = 0.8$ s to $t = 6.4$ s, r_1 decreases from $r_1 \approx 0.5r_0$ to $r_1 \approx 0.3r_0$, whereas r_2 increases from $r_2 \approx 1.6r_0$ to $r_2 \approx 2.1r_0$. The behavior of azimuthal velocity in the vortex in the range $r_1 < r < r_2$ (Fig. 4c) can be considered a kind of interpolation of the solutions obtained. It can be seen that the azimuthal velocity increases by three orders of magnitude during the time $t \approx 6$ s.

6. Numerical modeling of vortex dynamics in a convectively unstable atmosphere

The first attempts at analytic studies and numerical and laboratory modeling of vortices, including the effects related to the self-consistent dynamics of charged dust particles of various masses and electric charges, entrained by a hydrodynamical flow in an electrostatic field were made in Refs [107, 117, 132, 165–170]. However, studying vortex dynamics analytically in such a multi-component medium with the effect of electrostatic fields taken into account is presently a rather complicated task that continues to await its solution.

The influence of the vertical temperature gradient and friction in a surface layer on the dynamics of vortices was studied in Refs [52, 171–173]. By varying the values of parameters determining the initial vorticity, surface temperature, and friction in the surface layer, their influence on the maximum azimuthal velocity, pressure difference, and vortex structure was explored numerically. In [174], attention was focused on exploring the topology of DD vortices. The influence of charged dust particles and the evolving electric field on the dynamics of vortices was studied. Numerical modeling in Ref. [174] intended to solve two tasks: (1) to show that vortical motion is generated as a result of developing

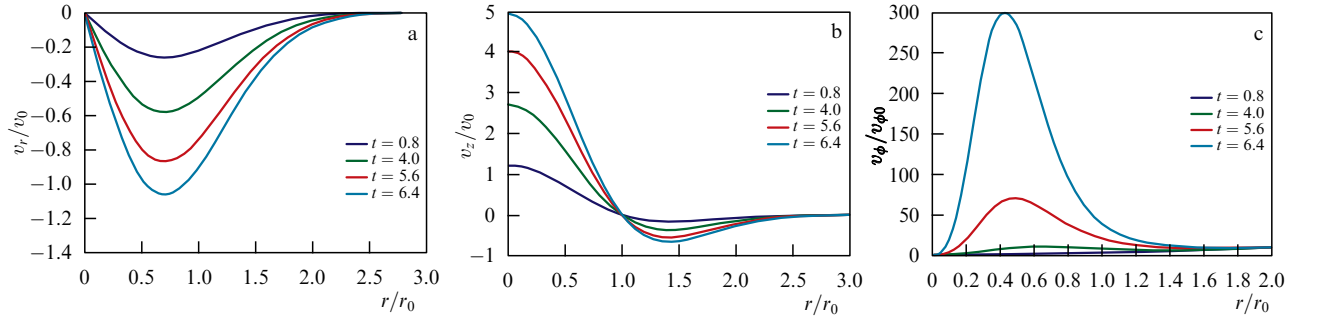

Figure 4. (Color online.) Normalized velocity components as functions of radius and time: (a) radial, (b) vertical, and (c) azimuthal.

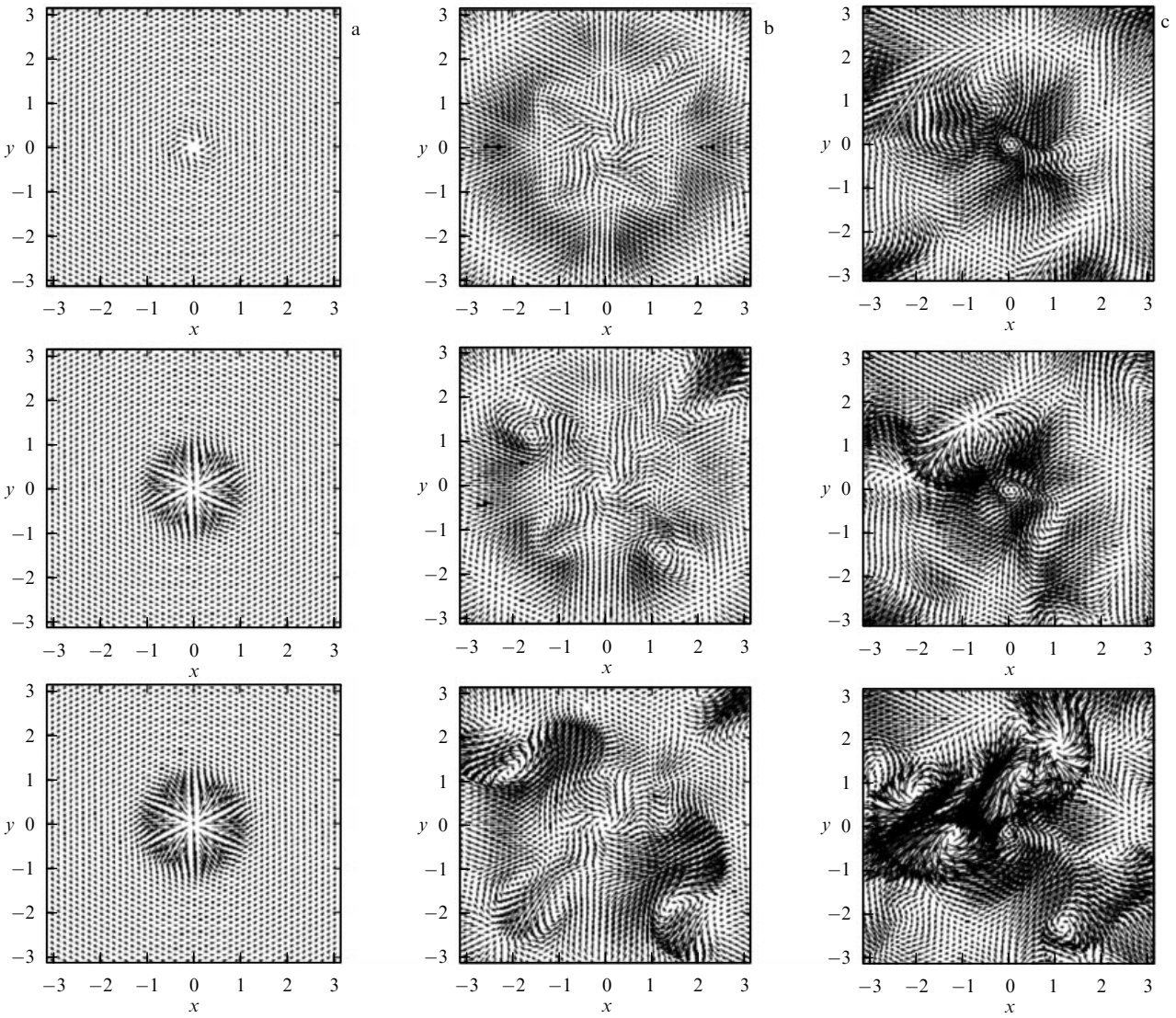

Figure 5. Results of numerical modeling of an isolated vortex in cross sections at different heights (the height (coordinate z) increases from top down in panels a–c) at the time instants (a) $t = 0$, (b) $t = 3.8$, and (c) $t = 4.8$.

convective instability; (2) to study the motion of individual sand particles entrained by a vortex. The system of Navier–Stokes equations in Cartesian coordinates in a compressible medium that was used consists of the continuity equation

$$\frac{\partial \rho}{\partial t} = -\frac{\partial(\rho v_j)}{\partial x_j}\,, \tag{58}$$

the momentum conservation equation

$$\frac{\partial \rho v_i}{\partial t} = -\frac{\partial(\rho v_i v_j)}{\partial x_j} - \frac{\partial p}{\partial x_j} + \frac{2}{\mathrm{Re}}\frac{\partial}{\partial x_j}\left(S_{ij} - \frac{1}{3}\,\delta_{ij}\frac{\partial v_j}{\partial x_j}\right) - \rho g\,\delta_{i3}\,, \tag{59}$$

and the equation for the total energy

$$\frac{\partial E_T}{\partial t} = -\frac{\partial}{\partial x_j}\left[(E_T + p)\,v_j\right] + \frac{1}{M^2\,\mathrm{Pr}\,\mathrm{Re}\,(\gamma_\mathrm{a} - 1)}\,\frac{\partial^2 T}{\partial x_j\,\partial x_j} + \frac{1}{\mathrm{Re}}\frac{\partial}{\partial x_j}\left[v_i\left(S_{ij} - \frac{1}{3}\,\delta_{ij}\frac{\partial v_j}{\partial x_j}\right)\right] - \rho v_3 g\,. \tag{60}$$

Here, $E_T = p/(\gamma_\mathrm{a} - 1) + 1/2\rho v_i^2$ is the energy density, $S_{ij} = 1/2(\partial v_i/\partial x_j + \partial v_j/\partial x_i)$, $\mathrm{Re} = V_0 L_0/\mu$ is the characteristic Reynolds number, V_0 and L_0 are the characteristic velocity and spatial scales, $\mathrm{Pr} = c_p\kappa/\mu$ is the Prandtl number, c_p is the specific heat at constant pressure, κ is the diffusivity coefficient, $M = V_0/c_0$ is the Mach number, c_0 is the speed of sound, and δ_{ij} is the Kronecker symbol.

Using the MUTSU/cNS3D (Multi Theoretical Subjects Utility/compressible Navier–Stokes 3D) code [175], the generation of vortices in a convectively unstable atmosphere was simulated numerically. The numerical code that was developed can be used in constructing models of general circulation in a dusty atmosphere. At the upper boundary, dissipation at constant pressure was imposed, with viscosity steadily increasing with height. The no-slip boundary conditions were applied at the lower boundary (the planet surface) for a given temperature distribution. In the initial state, the flow was imposed as a weak perturbation. The vertical velocity was assumed to be much smaller than the speed of sound. The first phase of modeling demonstrated the feasibility of azimuthal motion generation in an unstable poloidal flow under the conditions of convective instability. Figure 5a shows the velocity field at the initial instant $t = 0$ at different heights (increasing from top down). Figures 5b and c plot

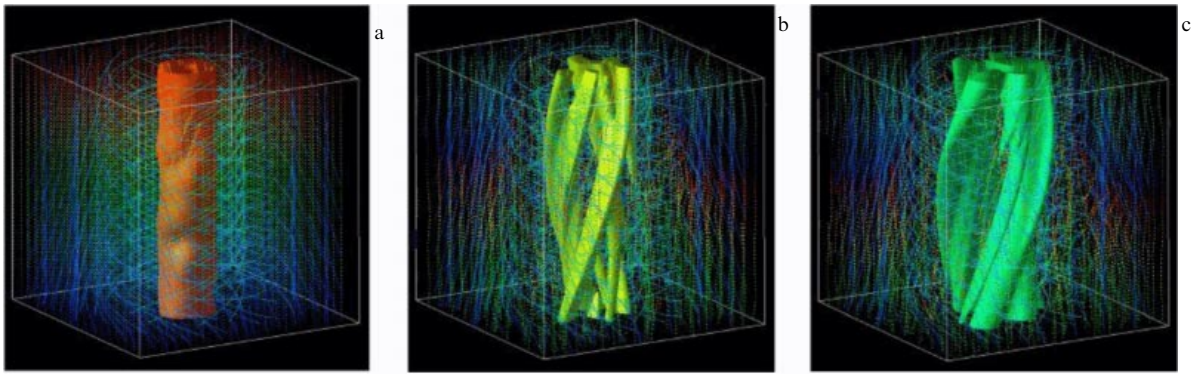

Figure 6. Three snapshots of vortex structure evolution; the time increases from panel a to c.

velocities at these heights at $t = 3.8$ and $t = 4.8$. The temporal dynamics shown in Fig. 5 explicitly indicate the existence of a nonlinear phase of convective instability. From Fig. 5c, it can also be seen that multivortex motion prevails at the nonlinear stage ($t = 4.8$). Thus, numerical simulations that were carried out point at the nonlinear stage of evolving convective instability, related to an increasing energy of toroidal motion.

In the second phase of numerical modeling, vertically periodic boundary conditions were used for a detailed study of the flow in the central part of DDs. For simplicity, temperature was assumed to be independent of the altitude. A pseudospectral code was used to study the evolution of the vortex structure. The dust component was treated as passive. Dust particles in Fig. 5 are shown as black points.

Figure 6 presents three snapshots from the evolution of the vortex structure (time increases from Fig. 6a to Fig. 6c). A vertically uniform flow was taken as the initial one in computations (Fig. 6a). Computations demonstrated that small-scale spiral structures form with time, from the snapshot shown in Fig. 6a (initial) to that shown in Fig. 6b. At later times, small-scale spiral structures decay, leading to the formation of a more symmetric central part in the transition from the snapshot in Fig. 6b to that in Fig. 6c. The time interval corresponds approximately to four DD rotations.

The snapshot in Fig. 6a shows a weak spiral structure, the snapshot in Fig. 6b shows a strong spirality, and the snapshot in Fig. 6c corresponds again to a weak spirality. Thus, inherent in the nonlinear dynamics of DDs are several characteristic frequencies of weakly chaotic vortical structure evolution.

7. Conclusions

We have summarized the results of observations, analytic studies, and the numerical modeling of CVs in the atmospheres of Earth and Mars. The focus is on studying analytic models of quasistationary structures and mechanisms generating CVs. From a popular class of CVs, dust devils are selected as the simplest vortices most actively discussed in the scientific literature. Considerable attention is devoted to the recently proposed model of CVs, characterized by a small set of parameters. Distinct from the Burgers and Sullivan vortices, which are exact vortical solutions of the Navier–Stokes equations, this model provides a description of structures bounded not only horizontally but also vertically. Stationary Burgers and Sullivan vortices form as a result of the balance of two effects: the concentration of vorticity in a converging radial flow and viscous diffusion of vorticity damping it.

The model discussed in this review corresponds to three-dimensional stationary incompressible motions of ideal fluid and is an exact solution of the Euler equations. In this model, the concentration of vorticity in a radial flow converging to the center is balanced by the transport of vorticity in the vertical direction. For an increasing height in the inner region, the vertical and azimuthal components of velocity also increase. At the height $z = L$, the vertical and azimuthal velocity components, together with the vertical vorticity, attain maximum values. In the upper part of the vortex, the upward flow converging to the center transforms into a downward and radially diverging flow. Such a model describes all characteristic features of CVs in their quasistationary evolution stage. The model allows computing vertical and radial fluxes of matter. In the new model, where the vertical and radial mass fluxes are equal to zero, $M_z = 0$ and $M_r = 0$, mass conservation is observed, whereas in the Burgers and Sullivan models, the vertical and radial mass fluxes grow without bounds with the height z and the distance from the symmetry axis.

Additionally, a nonlinear model for the generation of convective motions in CVs in an unstably stratified atmosphere is discussed. The model for the generation of convective cells — jets — is formulated in the axially symmetric approximation and involves nonlinear equations for internal gravity waves. It is shown that in a convectively unstable atmosphere with a large-scale seed vorticity, jets are rather rapidly transformed into intense vertical vortices. The temporal behavior of vertical vorticity and azimuthal velocity is described in the model by a double exponential, which corresponds to an explosive generation. The structure of the velocity field and vertical vorticity in such vortices is studied for the generation phase.

Further exploration of CVs, including numerical modeling, will allow (a) studying the generation and structure of generated vortices for arbitrary radial distances; (b) exploring the structure of vortices if the axial symmetry is broken; and (c) accounting for the effect of charged dust on the dynamics of vortices and the atmospheric dust content. Such research can help in studying and forecasting more powerful tornados and hurricanes, and in understanding the role of DDs and dust storms in the dynamics of atmospheric dust content.

Because of the rarefied atmosphere on Mars, Martian whirlwinds are much taller and more powerful than their terrestrial counterparts. The DDs on Mars can exceed their

terrestrial analogs by several hundred times. DDs, ejecting tons of electrically charged dust particles into the atmosphere of the planet, play an important role in the formation of climate. They may present a real danger to both robots and humans on the surface of the red planet. DDs can initiate lightning and electric discharges capable of destroying electronic instruments or interfering with radio transmissions. The next decades will witness an unprecedented number of autonomous instruments launched to Mars and, possibly, the first crewed mission. A clear understanding of physical processes taking place in Martian DDs is important for planning such missions.

The authors are indebted to M V Kurgansky, who made a number of valuable remarks, for a careful reading of the review, and to V G Bondur and I I Mokhov for the discussions and attention to this work.

The work was carried out in the framework of a state assignment to the Shmidt Institute of Physics of the Earth, Russian Academy of Sciences, a project of the Ministry of Education and Science of the RF, and a grant from the Russian Foundation for Basic Research, 18-29-21021mk.

References

1. Baddeley P F H *Whirlwinds and Dust-Storms of India* (London: Bell and Daldey, 1860)
2. Bagnold R A *The Physics of Blown Sand and Desert Dunes* (London: Methuen, 1941)
3. Nalivkin D V *Hurricanes, Storms, and Tornadoes. Geographic Characteristics and Geological Activity* (Rotterdam: A.A. Balkema, 1983); Translated from Russian: *Uragany, Buri i Smerchi. Geograficheskie Osobennosti i Geologicheskaya Deyatel'nost'* (Leningrad: Nauka, 1969)
4. Ives R L *Bull. Am. Meteor. Soc.* **28** 168 (1947)
5. Durward J *Nature* **128** 412 (1931)
6. "Weather overseas" *Weather* **4** 402 (1949)
7. Crozier W D *J. Geophys. Res.* **75** 4583 (1970)
8. Leovy C B *Nature* **424** 1008 (2003)
9. Balme M, Greeley R *Rev. Geophys.* **44** RG3003 (2006)
10. Vatistas G H, Kozel V, Mih W C *Exp. Fluids* **11** 73 (1991)
11. Church C R et al. *J. Atmos. Sci.* **36** 1755 (1979)
12. Howells P A C, Rotunno R, Smith R K *Q.J.R. Meteorol. Soc.* **114** 801 (1988)
13. Nolan D S, Farrell B F *J. Atmos. Sci.* **56** 2908 (1999)
14. Raasch S, Franke T *J. Geophys. Res.* **116** D16120 (2011)
15. Trapp R J, Fiedler B H *J. Atmos. Sci.* **52** 3757 (1995)
16. Idso S B *Bull. Am. Meteorol. Soc.* **56** 376 (1975)
17. Idso S B *Weather* **30** 115 (1975)
18. Rennó N O, Bluestein H B *J. Atmos. Sci.* **58** 927 (2001)
19. Sinclair P C, Ph.D. Thesis (Tucson, AZ: Univ. of Arizona, 1966)
20. Sinclair P C *J. Appl. Meteorol.* **8** 32 (1969)
21. Rankine W J M *A Manual of Applied Mechanics* (London: Charles Griffin and Co. Ltd, 1901)
22. Lorenz R D et al. *Space Sci. Rev.* **203** 5 (2016)
23. Kurgansky M V *Icarus* **300** 97 (2018)
24. Kok J F et al. *Rep. Prog. Phys.* **75** 106901 (2012)
25. Sinclair P C *Mon. Wea. Rev.* **92** 363 (1964)
26. Sinclair P C *Bull. Am. Meteorol. Soc.* **46** 388 (1965)
27. Lorenz R D, Myers M J *J. Meteorol.* **30** 178 (2005)
28. Sinclair P C *J. Atmos. Sci.* **30** 1599 (1973)
29. Ryan J A, Carroll I J *J. Geophys. Res.* **75** 531 (1970)
30. Fitzjarrald D E *J. Appl. Meteorol.* **12** 808 (1973)
31. Hess G D, Spillane K T *J. Appl. Meteorol.* **29** 498 (1990)
32. Metzger S M et al. *Geophys. Res. Lett.* **26** 2781 (1999)
33. Lewellen D C, Lewellen W S, Xia J *J. Atmos. Sci.* **57** 527 (2000)
34. Renno N O et al. *J. Geophys. Res.* **109** E07001 (2004)
35. Kurgansky M V *Dyn. Atmos. Oceans* **40** 151 (2005)
36. Kurgansky M V *Geophys. Res. Lett.* **33** L19S06 (2006)
37. Kurgansky M et al. *Space Sci. Rev.* **203** 209 (2016)
38. Carroll J J, Ryan J A *J. Geophys. Res.* **75** 5179 (1970)
39. Brian K et al. *Space Sci. Rev.* **203** 277 (2016)
40. Ringrose T J *Astron. Geophys.* **46** 5.16 (2005)
41. Thomas P, Gierasch P J *Science* **230** 175 (1985)
42. Ferri F et al. *J. Geophys. Res.* **108** 5133 (2003)
43. Balme M R, Whelley P L, Greeley R *J. Geophys. Res.* **108** 5086 (2003)
44. Tegen I, Lacis A A, Fung I *Nature* **380** 419 (1996)
45. Mahowald N *Science* **334** 794 (2011)
46. Mahowald N et al. *Annu. Rev. Environ. Resour.* **36** 45 (2011)
47. Yoshioka M et al. *J. Climate* **20** 1445 (2007)
48. Ramanathan V et al. *Science* **294** 2119 (2001)
49. Cakmur R V, Miller R L, Torres O *J. Geophys. Res.* **109** D07201 (2004)
50. Gu Z L et al. *Adv. Atmos. Sci.* **25** 31 (2008)
51. Onishchenko O G et al. *Climate* **7** 12 (2019)
52. Gobbi G P et al. *Atmos. Environ.* **34** 5119 (2000)
53. Ryan J A, Sharman R D, Lucich R D *Geophys. Res. Lett.* **8** 899 (1981)
54. Toon O B *Nature* **424** 623 (2003)
55. Twohy C H et al. *Geophys. Res. Lett.* **36** L01807 (2009)
56. Flanner M G et al. *Atmos. Chem. Phys.* **9** 2481 (2009)
57. Painter T H et al. *Proc. Natl. Acad. Sci. USA* **107** 17125 (2010)
58. Kohfeld K E, Harrison S P *Earth-Sci. Rev.* **54** 81 (2001)
59. Prospero J M, Lamb P J *Science* **302** 1024 (2003)
60. Murphy J et al. *Space Sci. Rev.* **203** 39 (2016)
61. Hess S L *Planet. Space Sci.* **21** 1549 (1973)
62. Smith P H et al. *Science* **278** 1758 (1997)
63. Klose M et al. *Space Sci. Rev.* **203** 377 (2016)
64. Ingersoll A P, Tryka K A *Science* **250** 435 (1990)
65. Jickells T D *Science* **281** 217 (1998)
66. Jickells T D et al. *Science* **308** 67 (2005)
67. Neakrase L D V et al. *Space Sci. Rev.* **203** 347 (2016)
68. Greeley R, Iversen J D *Wind as a Geological Process: on Earth, Mars, Venus, and Titan* (Cambridge: Cambridge Univ. Press, 1985)
69. Shao Y *Physics and Modelling of Wind Erosion* (Berlin: Springer, 2008)
70. Kurgansky M V *Icarus* **300** 97 (2018)
71. Aguirre C et al. *Aeolian Res.* **29** 12 (2017)
72. Lacks D J, Sankaran R M *J. Phys. D* **44** 453001 (2011)
73. Almeida M P et al. *Proc. Natl. Acad. Sci. USA* **10**5 6222 (2008)
74. Freier G D *J. Geophys. Res.* **65** 3504 (1960)
75. Lacks D J, Levandovsky A *J. Electrostat.* **65** 107 (2007)
76. Gill E W B *Nature* **162** 568 (1948)
77. Kok J F, Renno N O *Phys. Rev. Lett.* **100** 014501 (2008)
78. Kok J F, Renno N O *J. Geophys. Res.* **114** D17204 (2009)
79. Mills A A *Nature* **268** 614 (1977)
80. Schmidt D S, Schmidt R A, Dent J D *J. Geophys. Res.* **103** 8997 (1998)
81. Rudge W A D *Nature* **91** 31 (1913)
82. Stow C D *Weather* **24** 134 (1969)
83. Renno N O, Kok J F *Space Sci. Rev.* **137** 419 (2008)
84. Perkins S *Science* **353** 450 (2016)
85. Eden H F, Vonnegut B *Science* **180** 962 (1973)
86. Melnik O, Parrot M *J. Geophys. Res.* **103** 29107 (1998)
87. Harrison R G et al. *Space Sci. Rev.* **203** 299 (2016)
88. Izvekova Yu N, Popel S I *Plasma Phys. Rep.* **44** 835 (2018); *Fiz. Plazmy* **44** 747 (2018)
89. Izvekova Yu N, Popel S I *Contrib. Plasma Phys.* **56** 263 (2016)
90. Farrell W M et al. *J. Geophys. Res.* **109** E03004 (2004)
91. Farrell W M et al. *J. Geophys. Res.* **111** E01006 (2006)
92. Zheng X J, Huang N, Zhou Y-H *J. Geophys. Res.* **108** 4322 (2003)
93. Zhou Y-H, Guo X, Zheng X J *Phys. Rev. E* **66** 021305 (2002)
94. Huang N, Yue G, Zheng X *J. Geophys. Res.* **113** D20203 (2008)
95. Ireland P M *Powder Technol.* **198** 189 (2010)
96. Ireland P M *Powder Technol.* **198** 199 (2010)
97. Inculet I I, Castle G S P, Aartsen G *Chem. Eng. Sci.* **61** 2249 (2006)
98. Ireland P M, Jameson G J *J. Electrostat.* **71** 449 (2013)
99. Matsusaka S, Masuda H *Adv. Powder Technol.* **14** 143 (2003)
100. McGinnigle J B *Weather* **21** 272 (1966)
101. Mattsson J O, Nihlén T, Yue W *Weather* **48** 359 (1993)
102. Oke A M C, Tapper N J, Dunkerley D *J. Arid Environ.* **71** 201 (2007)
103. Kurgansky M V et al. *Bound.-Layer Meteorol.* **138** 285 (2011)
104. Ryan J A *J. Geophys. Res.* **77** 7133 (1972)

105. Snow J T, McClelland T M *J. Geophys. Res.* **95** 13707 (1990)
106. Balme M et al. *Geophys. Res. Lett.* **30** 1830 (2003)
107. Houser J G, Farrell W M, Metzger S M *Geophys. Res. Lett.* **30** 1027 (2003)
108. Tratt D M et al. *J. Geophys. Res.* **108** 5116 (2003)
109. Lorenz R D, Jackson B K *Space Sci. Rev.* **203** 277 (2016)
110. Greeley R et al. *J. Geophys. Res.* **108** 5041 (2003)
111. Stanzel C et al. *Geophys. Res. Lett.* **33** L11202 (2006)
112. Neakrase L D V et al. *Geophys. Res. Lett.* **33** L19S09 (2006)
113. Houghton J T et al. (Eds) *Climate Change 2001: the Scientific Basis: Contribution of Working Group I to the Third Assessment Report of the Intergovernmental Panel on Climate Change* (Cambridge: Cambridge Univ. Press, 2001)
114. Solomon S et al. (Eds) *Climate Change 2007: the Physical Science Basis: Contribution of Working Group I to the Fourth Assessment Report of the Intergovernmental Panel on Climate Change* (Cambridge: Cambridge Univ. Press, 2007)
115. Gillette D A, Sinclair P C *Atmos. Environ. A* **24** 1135 (1990)
116. Crozier W D *J. Geophys. Res.* **69** 5427 (1964)
117. Farrell W M et al. *Geophys. Res. Lett.* **30** 2259 (2003)
118. Farrell W M et al. *J. Geophys. Res.* **111** E01006 (2006)
119. Farrell W M et al. *J. Geophys. Res.* **109** E03004 (2004)
120. Esposito F et al. *Geophys. Res. Lett.* **43** 5501 (2016)
121. Ryan J A *J. Geophys. Res.* **69** 3759 (1964)
122. Neubauer F M *J. Geophys. Res.* **71** 2419 (1966)
123. Gierasch P, Goody R M *J. Atmos. Sci.* **30** 169 (1973)
124. Ryan J A, Lucich R D *J. Geophys. Res.* **88** 11005 (1983)
125. Golombek M et al. *Science* **278** 1743 (1997)
126. Schofield J T et al. *Science* **278** 1752 (1997)
127. Malin M C, Edgett K S *J. Geophys. Res.* **106** 23429 (2001)
128. Stanzel C et al. *Icarus* **197** 39 (2008)
129. Petrosyan A et al. *Rev. Geophys.* **49** RG3005 (2011)
130. Fenton L K, Lorenz R *Icarus* **260** 246 (2015)
131. Whelley P L, Greeley R *J. Geophys. Res.* **111** E10003 (2006)
132. Lacks D J *Nat. Phys.* **6** 324 (2010)
133. Xie L, Ling Y, Zheng X *J. Geophys. Res.* **112** D12116 (2007)
134. Zelenyi L M et al. *Solar Syst. Res.* **49** 509 (2015); Translated from Russian: *Vestn. Nauch. Proizv. Ob'ed. im. S A Lavochkina* (2) 13 (2014)
135. Balme M R, Hagermann A *Geophys. Res. Lett.* **33** L19S01 (2006)
136. Burgers J M *Adv. Appl. Mech.* **1** 171 (1948)
137. Rott N *Z. Angew. Math. Phys.* **9** 543 (1958)
138. Sullivan R D *J. Aerospace Sci.* **26** 767 (1959)
139. Dolzhanskii F V, Krymov V A, Manin D Yu *Phys. Usp.* **33** 495 (1990); *Usp. Fiz. Nauk* **160** (7) 1 (1990)
140. Onishchenko O G, Pokhotelov O A, Astafieva N *Phys. Usp.* **51** 577 (2008); *Usp. Fiz. Nauk* **178** 605 (2008)
141. Williams N R *Bull. Am. Meteorol. Soc.* **29** 106 (1948)
142. Battan L J *J. Meteorol.* **15** 235 (1958)
143. Bluestein H B, Weiss C C, Pazmany A L *Mon. Wea. Rev.* **132** 209 (2004)
144. Toigo A D et al. *J. Geoghys. Res.* **108** 5047 (2003)
145. Zhao Y Z et al. *Atmosphere-Ocean* **42** 61 (2004)
146. Krasnov Y K, Kiknadze G I *Sov. Phys. Dokl.* **31** 799 (1986); *Dokl. Akad. Nauk SSSR* **290** 1315 (1986)
147. Davies-Jones R *Atmos. Res.* **158–159** 274 (2015)
148. Onishchenko O G, Pokhotelov O A, Astafieva N M *Izv. Atmos. Oceanic Phys.* **54** 130 (2018); Translated from Russian: *Geofiz. Protsessy Biosfera* **17** 61 (2018)
149. Onishchenko O et al. *J. Geophys. Res. Atmosp.* **121** 11264 (2016)
150. Onishchenko O G et al. *J. Fluid Mech.* (2019), submitted
151. Morton B R *J. Fluid Mech.* **38** 315 (1969)
152. Smith R K, Montgomery M T, Persing J *Q.J.R. Meteorol. Soc.* **140** 2638 (2014)
153. Rennó N O, Burkett M L, Larkin M P *J. Atmos. Sci.* **55** 3244 (1998)
154. Rennó N O et al. *J. Geophys. Res.* **105** 1859 (2000)
155. Fritts D C, Alexander M J *Rev. Geophys.* **41** 1003 (2003)
156. Mitchell N J, Howells V St C *Ann. Geophys.* **16** 1367 (1998)
157. Rafkin S et al. *Space Sci. Rev.* **203** 183 (2016)
158. Stenflo L *Phys. Lett. A* **222** 378 (1996)
159. Onishchenko O G, Pokhotelov O A *Dokl. Earth Sci.* **445** 845 (2012); *Dokl. Ross. Akad. Nauk* **445** 86 (2012)
160. Onishchenko O, Pokhotelov O, Fedun V *Ann. Geophys.* **31** 459 (2013)
161. Onishchenko O G et al. *Ann. Geophys.* **32** 181 (2014)
162. Onishchenko O G, Pokhotelov O A, Fedun V *Dokl. Earth Sci.* **454** 37 (2014); *Dokl. Ross. Akad. Nauk* **454** 89 (2014)
163. Onishchenko O G et al. *Phys. Scr.* **89** 075606 (2014)
164. Onishchenko O G et al. *Phys. Scr.* **90** 068004 (2015)
165. Myhre G, Stordal F *J. Geophys. Res.* **106** 18193 (2001)
166. Kamra A K *J. Geophys. Res.* **77** 5856 (1972)
167. Gu Z L, Wei W, Zhao Y *Aerosol Air Qual. Res.* **10** 272 (2010)
168. Kanak K M, Lilly D K, Snow J T *Q.J.R. Meteorol. Soc.* **126** 2789 (2000)
169. Kanak K M *Q.J.R. Meteorol. Soc.* **131** 1271 (2005)
170. Jackson T L et al. *J. Geophys. Res.* **115** E05006 (2010)
171. Miura H, Kida S *J. Phys. Soc. Jpn.* **63** 4000 (1994)
172. Miura H *Comput. Phys. Commun.* **147** 552 (2002)
173. Miura H *J. Turbul.* **5** (1) 010 (2004)
174. Horton W et al. *J. Geophys. Res.* **121** 7197 (2016)
175. Miura H, Nakajima N *Nucl. Fusion* **50** 054006 (2010)